Electrochimica Acta 461 (2023) 142660

Contents lists available at ScienceDirect

Electrochimica Acta

journal homepage: www.journals.elsevier.com/electrochimica-acta

Suppressing water migration in aqueous Zn-iodide flow batteries by asymmetric electrolyte formulation

Monalisa Chakraborty [a,b,*], Teresa Andreu [c,d,**], Ben Molinari [a], Joan R. Morante [a,c,d], Sebastián Murcia-López [a]

[a] Catalonia Institute for Energy Research (IREC), Jardins de les Dones de Negre 1, Sant Adrià de Besós 08930, Spain
[b] Universitat Autonoma de Barcelona (UAB), Plaça Cívica, Bellaterra 08193, Spain
[c] Universitat de Barcelona (UB). Martí i Franquès 1, Barcelona 08028, Spain
[d] Institut de Nanociència i Nanotecnologia (IN2UB), Martí i Franquès 1, Barcelona 08028, Spain

ARTICLE INFO

Keywords:
Zinc-iodide
Redox flow batteries
Electrolyte
Water migration

ABSTRACT

Zinc-iodide flow battery (ZIFB) is under research for the last years due to its suitability as a potential candidate for future electrochemical energy storage. During cycling, one of the biggest challenges that affect the reliable performance of ZIFB is the substantial water migration through the membrane because of differential molar concentrations between anolyte and catholyte that imbalance the osmotic pressures in each compartment. Considering the mass balances, herein we propose to equalize the total ionic concentration of electrolytes by the addition of extra solute into the compartment of lower ion concentration as a way to restrict the water crossover. Experimental validation of this electrolyte concentrations balancing strategy has been carried out by assessing the post-cycled electrolytes, and half-cell charged electrolytes, which confirms the efficient suppression of water migration from catholyte to anolyte. Besides, in-depth analysis of ions and water transport mechanism through Nafion 117 membrane confirms that solvated K^+ ions of lower ionic radius compared to solvated Zn^{2+} ions, are the dominant migrating carrier. Therefore, the addition of extra KI solute is beneficial to suppress the major transport of large hydrated Zn^{2+} ions along with the higher amount of water. Finally, the improved ZIFB cell behaviour with enhanced electrical conductivity, discharge capacity, and voltage efficiency in the cell assembled with the electrolytes of balanced molar concentrations concludes our present study, proving that tuning the electrolytes concentrations is an effective way to suppress water migration as an appealing method in the prospect of upscaling ZIFB application.

1. Introduction

Redox flow batteries (RFBs) are considered as one of the most promising stationary large-scale energy storage technologies, significantly for the integration with renewable energies [1–4]. Despite all-vanadium RFBs, owing to their impressive cycle life, good electrochemical reversibility, are the most developed RFBs till date [4–7], their large-scale deployments are still confronted challenges, for example, limitation of low energy density (~ 25 $W{\cdot}h{\cdot}L^{-1}$), the low solubility of active species in the aqueous solution [8] and growing cost of vanadium due to uprising global demand. Hence, to meet the global demand for energy storage systems as well as maintaining as a further contender to store renewable energies, alternative flow battery technologies are under investigation. Zinc-based aqueous RFBs, hold great promise for next-generation FBs applications due to their appealing features of cost-effectiveness, high safety, and high energy density [9]. Over the several novel redox chemistries, Zn/Zn^{2+} (negative) | I^-/I_3^- (positive) redox couple have gained high interest due to its non-toxic and less corrosive features, unlike Br^-/Br_2 chemistry [10–18]. B.Li et al. firstly proposed an ambipolar zinc-iodide flow battery (ZIFB) based on a near-neutral ZnI_2 aqueous electrolyte, with a high discharge energy density of 167 $W{\cdot}h{\cdot}L_{catholyte}^{-1}$, nearly seven times that of the state-of-the-art vanadium RFB and approaching the energy density of $LiFePO_4$-based Li-ion battery [10].

The ZIFB is operated based on the following electrochemical redox reactions:

* Corresponding author at: Catalonia Institute for Energy Research (IREC), Jardins de les Dones de Negre 1, Sant Adrià de Besós 08930, Spain
** Corresponding author at: Universitat de Barcelona (UB). Martí i Franquès 1, Barcelona 08028, Spain.
E-mail addresses: moncha@kth.se (M. Chakraborty), tandreu@ub.edu (T. Andreu).

https://doi.org/10.1016/j.electacta.2023.142660
Received 10 September 2022; Received in revised form 1 May 2023; Accepted 25 May 2023
Available online 26 May 2023

Anode:

$$Zn_{(s)} \leftrightarrow Zn^{2+}_{(aq)} + 2e^- \quad (E^0 = -0.76\ V_{SHE}) \tag{1}$$

Cathode:

$$2I^-_{(aq)} \leftrightarrow I_{2(s)} + 2e^- \tag{2}$$

$$I_{2(s)} + I^-_{(aq)} \leftrightarrow I^-_{3(aq)} \tag{3}$$

$$I^-_{3(aq)} + 2e^- \leftrightarrow 3I^-_{(aq)} \ (E^0 = 0.54\ V_{SHE}) \tag{4}$$

Overall reaction:

$$I^-_{3(aq)} + Zn_{(s)} \leftrightarrow 3I^-_{(aq)} + Zn^{2+}_{(aq)} \ (E^0 = 1.30\ V) \tag{5}$$

The general schematic of ZIFB was already mentioned in our previous publication [18] pointing out the suitability of this system to be integrated with efficient photoelectrodes for next-generation solar charging batteries. During the charge process, metallic Zn Eq. (1)) is reductively electrodeposited on the anode surface while iodide (I^-) ion is oxidized to iodine (I_2), which is further complexed with an I^- ion to form soluble triiodide (I_3^-) species (Eqs. (2)-(4)) in the positive side of the cell. The reverse process occurs upon discharge.

Nevertheless, in ZIFBs, several challenges need to be addressed before reaching their full promising potentials, such as extending battery discharge capacity following cycle life by ameliorating irreversible metallic Zn plating/stripping on the anode and suppressing water migration from one compartment to another during cycling. Different approaches have already been reported to address some of these challenges, such as enhancing the energy efficiency by introduction of MOF-based electrocatalyst [11] modifying electrolyte composition via incorporation of bromide ions [12] and chloride ions [19] as complexing agents, tuning the anolyte pH [20], replacing ZnI_2 electrolyte by KI and $ZnBr_2$ along with the introduction of low-cost porous separator with self-healing mechanism from Zn dendrite growth [13].

Therefore, water migration during cycling is a concerning issue in all flow batteries chemistries, which need to be addressed for the prospect of capacity retention, cyclability, and long-term stability. In all-vanadium RFBs, several groups have reported this issue for the last decade. Sun and co-workers first investigated the source of water migration in VRFBs. They have mentioned that the concentration differences of vanadium ions between positive and negative compartments are the main reason for the ion crossover along with the water transfer driven by osmosis and electro-osmotic drag (EOD) through the Nafion proton exchange membrane [21]. Knehr et al. have presented a mathematical 2-D transient, isothermal model of a VRFB which incorporates the species crossover as well as the transfer of water across the membrane, resulting in cell capacity loss [22]. Yan et al. have demonstrated the mechanism of restricting the electrolyte volume changes through balancing the osmotic pressure via the addition of a draw solute of 2-methylimidazole in the electrolyte of a single-cell VRFB assembled with TiO_2 nanoporous membrane [23]. Oh et al. have developed a water transport model which accounts for the various mechanisms of water and species crossover through the membrane. Further, they have validated this numerical model with experimental data and found that the water crossover via diffusion and EOD are the dominant mechanisms that cause electrolyte imbalance during cell charging/discharging [24]. Song and co-workers have also studied electrolyte transfer mechanisms across a Nafion membrane based on the transport phenomena and further validated experimentally, where they found the electrolyte imbalance during cycling as the effect of viscosity, which they have optimized by manipulating the flow rate [25].

Apart from the vanadium redox chemistry, Liu group has addressed the water migration in alkaline Zn-Fe FBs. They have found that the water migration is the combined effect of concentration gradient, ionic strength difference on half-cell electrolytes and the electric field. For mitigation purposes, they have studied a series of electrolyte additives and observed that Na_2SO_4 as an additive in the negative electrolyte is showing a good performance by suppressing water migration of Zn-Fe FB cell assembled with polybenzimidazole membrane [26]. Mousavi et al. have reported that differential hydraulic pressure between two sides of the microporous polyethylene separator, accelerates electrolyte transport as well as species crossover via convection, which they have optimized theoretically and experimentally by maintaining asymmetric half-cell electrolyte flow rates in a ZIFB single-cell [16].

So far, it is clear from the literature that water migration during flow batteries operation is a serious challenge, normally overlooked, that can cause efficiency decay in long-term cycling, and hinder flow batteries from the large-scale deployment. Most of the studies have been reported based on numerical water transport models to understand the transport mechanism [14–16].

Few studies have been done so far on single-flow ZIFBs to restrict water transfer between compartments. For example, Xie et al. described a high-power density single-flow ZIFB by sealing the positive compartment [14]. Ito et al. reported <90% coulombic efficiency after the addition of propylene carbonate in the electrolyte, forming hydrophobic polyiodide complex during cathodic oxidation in a single-flow ZIFB without cation exchange membrane [15].

Herein, we propose to formulate an asymmetric redox flow battery to compensate ion migration by the addition of extra solute to the catholyte as a simple strategy to restrict water migration.

2. Materials and methods

2.1. ZIFB single-cell

The assembling of ZIFB single cell has been described in detail in our previous publication [18]. Electrodes of 10 cm^2 geometric area were assembled by sandwiching commercial CEM Nafion® 117 in between anode and cathode compartments. The membrane was pre-treated in 3% H_2O_2, H_2O, and 0.5 M H_2SO_4 at 80℃ for 1 hour in each step respectively. Graphite foil (Alfa Aesar®, 0.5 mm thick) and graphite felt (Sigracell® GFA 1.5 EA, 1.5 mm thick) were used as anode and cathode respectively. Graphite felt was thermally pre-treated at 420°C for 10 hours with a ramp rate of 5°C·min^{-1} in air. A titanium metal plate was used as a negative current collector. Around 4 mm space was kept between the anode surface and membrane for the solid Zn plating. A graphite plate was used as a positive current collector. An aqueous solution containing a mixture of 1.5 M ZnI_2 (98.0%, Aldrich) and 1.5 M KI (99.5%, Sigma Aldrich) (1:1) was used as the standard electrolytes in both cell chambers and after the addition of extra 2 M KI in the catholyte, the electrolyte ratio was 1.5:3.5 in the catholyte chamber. Electrolytes were prepared at room temperature by mixing in Milli-Q ultrapure water. The cell was connected to two glass cylinders (10 mL of electrolyte on each reservoir) to measure the volume changes of electrolytes during charge/discharge operation. Electrolyte was circulated to the cell by a peristaltic pump (Masterflex L/S series) through Tygon® tubing at a fixed flow rate of 13 mL·min^{-1}.

The electrochemical charge-discharge test of ZIFB single cell was conducted under galvanostatic conditions operating at current densities of 10 and 20 mA·cm^{-2} respectively, as representative in the design of solar-powered electrochemical devices [27]. The charge was controlled by both upper cut-off voltage (1.6 V) and 67% of theoretical capacity (based on preliminary calculations) [18]

2.2. Designing of the cell set-up for in-situ electrochemical analysis

The schematic of strategically designed cells set-up for the in-situ electrochemical study is represented in Fig. S1 (practical set-up after assembling is shown in Fig. S2). ZIFB single cell as described in Section 2.1, is connected with these two identical, auxiliary cells in series. These identical cells were built for performing in-situ electrochemical impedance (EIS) of half-cell electrolytes. The components details are described

in Fig. S3. These auxiliary cells are made up of graphite foil as working electrode and graphite felt as counter/reference electrode of 4 cm^2 electrode geometric areas, without a separator/membrane. Graphite foil and graphite felt are the same as used in the ZIFB single cell. Each half-cell electrolyte passed through the ZIFB single cell which then entered into these auxiliary cells, finally flowing out from the auxiliary cells to the reservoirs. Graphite plates with serpentine flow frames are used as current collectors.

Through this setup, changes in the half-cell electrolytes resistance were analyzed in real-time by applying potentiostatic electrochemical impedance spectroscopy (PEIS) on electrolytes at different state of charge (SOC) passing through the two auxiliary half-cells. Electrolytes were charged from 0 to 60% SOC with intervals of 15%. In between, PEIS was conducted in open-circuit conditions (OCV) within a frequency range of 200 kHz to 100 mHz and AC perturbation of 10 mV of amplitude. The complete measurement was carried out at the 1st charging cycle of the ZIFB single cell at the current density of 10 $mA{\cdot}cm^{-2}$.

In addition, the current-interrupt method was used to evaluate the changes of the ohmic resistance (R_{ohm}) of the ZIFB full-cell at the aforementioned SOC%. This technique, frequently applied in the fuel cells, is based on the transient voltage response after current interruption (i.e. changing from polarization conditions to the relaxation mode in a short period) [28]. The estimation method is detailed in the supporting information (Fig. S6) in brief.

2.3. Migration of cations through Nafion membrane

Cation migration through Nafion 117 cation-exchange membrane (CEM) test was analyzed by using anolyte and catholyte solutions. The ZIFB cell was charged up to 67% of theoretical capacity at 20 $mA{\cdot}cm^{-2}$ of current density by keeping the same conditions mentioned in Section 2.1. Anolyte and catholyte solutions collected at 0% and 67% SOCs of both the cases: with and without extra added 2 M KI were analyzed with ICP-OES (Perkin Elmer Optima 3200 RL) to determine the Zn^{2+} and K^+ ions concentrations. Concentrations of Zn^{2+} ions were measured at the corresponding wavelengths of 202, 206, and 213 nm, and the average value is displayed in Table S5, and 766 nm of wavelength was applied to measure the concentrations of the K^+ ions.

3. Results and discussion

3.1. Electrolytes volume imbalance post cycling

In a standard redox ZIFB, both anolyte and catholyte have the same electrolyte composition. In line with our former work [18] the standard electrolyte was an aqueous solution of 1.5 M ZnI_2 and KI (1:1 ratio). Upon cycling, we have observed the above-mentioned water migration issue. As a representative example, in Fig. S4 it can be seen the electrolyte volumes after 15 charge-discharge galvanostatic cycles at 20 $mA{\cdot}cm^{-2}$ of a ZIFB single cell. Considering that the initial volume at each compartment was 10 mL, the volume of the anolyte increased from the initial state while the catholyte is showing an intense reduction from the initial volume, causing an imbalance, with a partially irreversible water transfer from catholyte to anolyte upon cycling.

The reason for water transfer might be attributed to the effect of the imbalance of ionic concentrations between anolyte and catholyte compartments. As stated by several groups [16,21,23–26] multiple factors such as combined effects of concentration gradient, difference in the ionic strength, hydraulic pressure, and viscosity, crucially affect water crossover through a membrane via diffusion; EOD or osmosis mechanism. During charge, the number of free active anions and cations, I^- in catholyte and Zn^{2+} in anolyte, decrease due to the formation of I_3^- species and solid Zn electroplating, respectively, together with the subsequent movement of cations through the Nafion membrane to balance the charges between the two half-cells.

In our case, the anolyte and catholyte (at 0% SOC) are made up of 1.5 $mol{\cdot}L^{-1}$ ZnI_2 and KI (1:1), hence, having identical numbers of the total concentrations of ions of 7.5 $mol{\cdot}L^{-1}$ on both sides. During the charging process, considering electroplating of 1 $mol{\cdot}L^{-1}$ Zn^{2+} on the anode while 3 $mol{\cdot}L^{-1}$ of I^- will produce 1 $mol{\cdot}L^{-1}$ I_3^- in the cathode side. Consequently, at 67% SOC, the total concentration of ions is 6.5 $mol{\cdot}L^{-1}$ in anolyte and 5.5 $mol{\cdot}L^{-1}$ in catholyte. When Nafion CEM is used as the separator for ZIFB, cations (Zn^{2+} and K^+ along with H^+) are the main charge-balancing ions. Therefore, to balance the charges, based on the following electroneutrality condition in the electrolyte:

$$\sum_i z_i c_i^e = 0 \tag{6}$$

respective Zn^{2+} and K^+ ions will migrate from catholyte to anolyte, resulting in differential ions concentrations of 8 $mol{\cdot}L^{-1}$ and 4 $mol{\cdot}L^{-1}$ in anolyte and catholyte respectively, as seen in Table S1. Because of differential ions concentrations between two compartments, water shuttle takes place from the chamber of lower ionic concentration (catholyte) to the higher ionic concentration (anolyte) via the osmosis phenomenon.

In order to further understand the real-time variations during the charge, electrolyte resistances have been measured using auxiliary cells coupled in series to the electrolyte circuit (Figs. S2–S3). Fig. 1 represents half-cell EIS analysis of electrolytes, in the course of first charging at various SOCs (from 0% to 60% SOC). In the impedance analysis of anolyte (Fig. 1a) of standard electrolyte, it could be seen that charge transfer resistance (R_{ct}) is decreasing with an increment of SOC, from 153 $\Omega{\cdot}cm^2$ at 0% SOC to 74 $\Omega{\cdot}cm^2$ at 60% SOC (fitted from the aforementioned Randles equivalent circuit). This descending trend of R_{ct} might be caused by the gradual decrement of Zn^{2+} ions concentration in the anolyte during charge which is partially compensated by K^+ ions perturbing the spatial double layer. On the other hand, ohmic resistance (R_{ohm}) decreases from 7.8 $\Omega{\cdot}cm^2$ to 4.0 $\Omega{\cdot}cm^2$ as SOC increases from 0% to 60%. This decreasing trend could be visible in the onset enlarged plot. The decrement of R_{ohm} is equally attributed by the partial replacement of Zn^{2+} by K^+ ions with higher ionic mobility.

At the cathode side (Fig. 1b) ohmic resistance (R_{ohm}) exhibits a rising trend from 4.5 $\Omega{\cdot}cm^2$ to 7.4 $\Omega{\cdot}cm^2$ with higher SOC, 0 to 60% respectively. As per Eq. (4), in the charging process, 3 moles of I^- are oxidized to produce 1 mol of I_3^- together with the cation migration to the anolyte side, limiting the number of free charge carriers, hence, increasing catholyte ohmic resistance. Concerning charge transfer resistance, upon charging it was observed a slight decrement of R_{ct} from 8.3 $\Omega{\cdot}cm^2$ to 4.8 $\Omega{\cdot}cm^2$. The reason for this decreasing trend might be correlated with the statement given by Jeon and co-workers, where they have studied the effect of charge transfer resistance, electrode kinetics through in-situ EIS analysis in the catholyte and anolyte respectively in zinc-bromine redox flow batteries. A similar reduction of R_{ct} in catholyte has been observed which is explained by the formation and further accumulation of polybromide complexes on the cathode surface. These accumulated polybromide complexes promote the electrochemical adsorption of the Br^-, hence, accelerating the overall electrode reaction and reduction of R_{ct} with increasing SOC [29] Similar roles of $I_3^-/I_2/I^-$ halide chemistry could be hypothesized from our catholyte EIS analysis, where charged I_3^- species play a positive role in the adsorption of I^- ion at the double layer interface, facilitating the reduction of the R_{ct} at high SOC.

3.2. Mitigation strategy

Based on the above analysis on the water migration from catholyte to the anolyte via osmosis as an effect of differential ionic concentrations, 2 $mol{\cdot}L^{-1}$ of KI are added as an extra solute to the catholyte to balance the total concentrations of ions in both compartments at 67% SOC (Table S2). Hence, now, at 0% SOC, total concentrations of ions of anolyte and catholyte are 7.5 $mol{\cdot}L^{-1}$, 11.5 $mol{\cdot}L^{-1}$, respectively. After charging process by considering electroplating of 1 $mol{\cdot}L^{-1}$ Zn^{2+} and

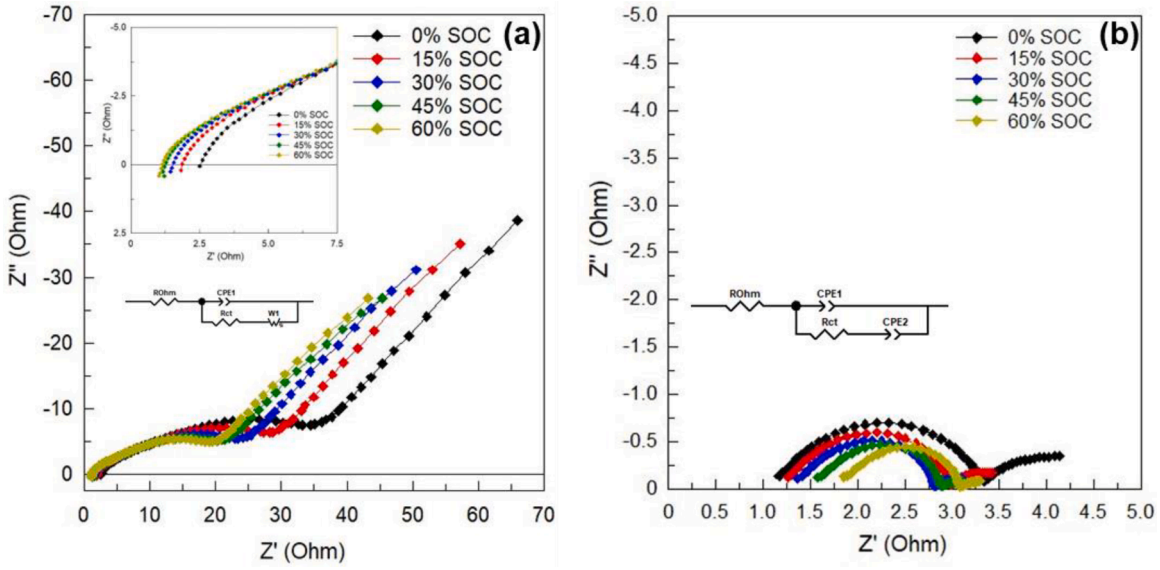

Fig. 1. In-situ electrochemical impedance spectroscopy (EIS) analysis of half-cell electrolytes under various SOCs for the 1st cycle of charge at a current density of 10 mA·cm^{-2}. (a) anolyte and (b) catholyte with 1.5 M ZnI_2: KI (1:1). (the inset shows the equivalent circuit model used to fit the experimental data).

formation of 1 mol·L^{-1} I_3^-, the total concentration of ions is 6.5 mol·L^{-1} in anolyte and 9.5 mol·L^{-1} in catholyte. Afterward, the migrations of Zn^{2+} and K^+ cations for charge neutrality, the total concentrations of ions reach a balanced state of the identical value of 8 mol·L^{-1} in each chamber unlike the previous electrolyte of values 8 mol·L^{-1} in anolyte and 4 mol·L^{-1} in catholyte.

To get the practical insight of water migration mechanism as an effect of differential ions concentrations and amelioration by balancing the total number of ions in both compartments after addition of extra solute to the catholyte, ZIFB cell was cycled with 1.5 M ZnI_2:KI (1:1) anolyte, and with 1:1 and 1.5: 3.5 ratios in the catholyte at 20 mA·cm^{-2}. Fig. 2a represents the volume variations of half-cell electrolytes after 1st charge cycle of cases: without and with added 2 M KI in the catholyte. At the 1st charged state, these two sets of electrolytes depict a well-clear difference in volume. The cell operated with the standard 1:1 ratio catholyte, shows ~3.75 mL of water transfer from catholyte to anolyte, whereas the cell ran with added extra KI presents comparatively less water shuttle of ~1.25 mL. The optical images of half-cell electrolytes (Fig. S5a-f) before and after charge depict the real-time picture of water migration. Overall, this comparison of the half-cell electrolytes volume changes in two cases justifies the hypothesis explained of suppressing water migration by balancing the total concentration of ions between two chambers. Furthermore, the volume of half-cell electrolytes after 15 continuous cell charge-discharge cycles with tuned electrolytes is illustrated in the bar graph of Fig. 2b. Besides, volume after discharge of half-cell electrolytes in certain cycles is shown in Fig. S6a. Unlike the volume variations trend with the cell operated with standard electrolyte, here, the trend is not that similar of extreme decrement of catholyte volume and increment of anolyte volume despite a way less reduction of catholyte volume (~2 mL). Optical images of cycled electrolytes in Fig. S6b-c, present almost the same electrolyte volumes, with minor electrolyte pumping losses [30], adding another evidence of suppressed water transfer from catholyte to anolyte as a real-time view.

The measurement using the auxiliary cells revealed a more stable ohmic resistance of both compartments in the asymmetric electrolyte formulation compared to the standard cell, as shown in Fig. 3. The addition of extra KI at the catholyte compensates the ohmic resistance increment due to the depletion of I^- and K^+ ions during the charge process, corroborating our initial hypothesis. On the other hand, the reduction of ohmic resistance at the anolyte is unavoidable due to the replacing of Zn^{2+} by K^+ ions and the differences between both configurations might be attributed to the effective ion concentrations and mobilities owing to the fact that water is also migrating to the anolyte side.

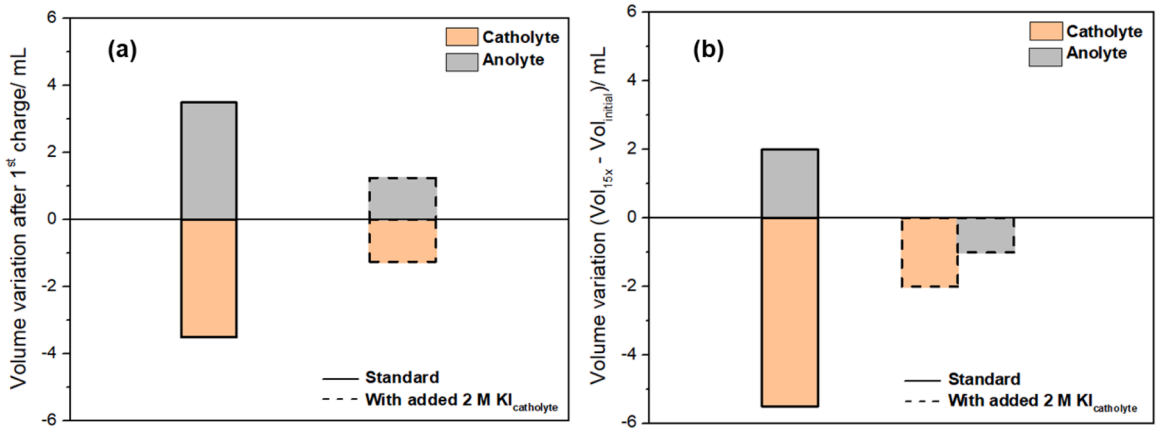

Fig. 2. Volume variations of electrolytes after ZIFB full-cell cycling at a current density of 20 mA·cm^{-2}. (a) after 1st charge cycle and (b) after 15th charge-discharge cycles of electrolyte 1.5 M ZnI_2: KI (1:1) + 2 M $KI_{catholyte}$.

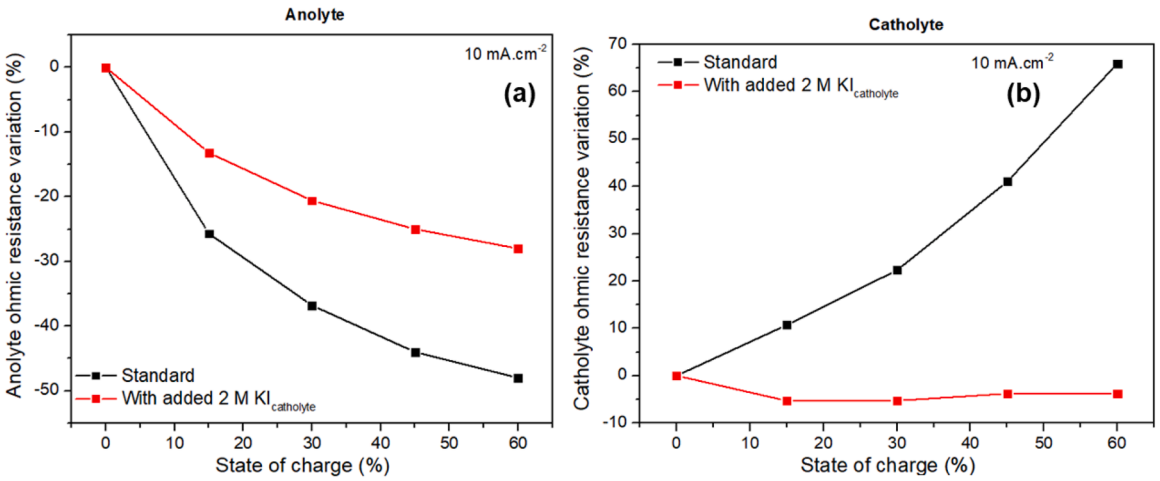

Fig. 3. Comparison of the variations of (a) anolyte, and (b) catholyte ohmic resistances (R_{ohm}) with various SOCs for both electrolyte formulations (data reported in Table S3 in the supporting information).

3.3. *Mass transport through the membrane*

To corroborate that the ion transport through the Nafion membrane influences the water crossover during charge, Zn^{2+} and K^{+} ions concentrations were determined by ICP-OES. Measurements were done with standard 1:1 catholyte, and tuned 1.5:3.5 catholyte at 0% and 67% SOC. Concentrations of I^{-} and I_3^{-} ions are estimated from the faradaic equations based on the Zn^{2+} and K^{+} ions concentrations. The mass balance to analyse the ion transport through the membrane was calculated taking into account the molar concentrations and the actual volume of each compartment due to water migration (Tables S4, S5). As seen in Table S5, the number of moles of I^{-} ions in anolyte, before and after the charged state of both, the standard and tuned electrolyte, shows well evidence of no migration of anions through Nafion 117.

The standard electrolyte is having identical number of moles of Zn^{2+} and K^{+} ions before charge. From the differences in the number of moles of K^{+} ions in anolyte and catholyte, before and after charge, it is estimated that ~85% of K^{+} ions moved from catholyte to anolyte through the membrane. On the other side, the differences of Zn^{2+} ions in anolyte and catholyte indicate that ~63% of Zn^{2+} ions moved from catholyte to anolyte in the charging process. Whereas the tuned electrolyte with extra added 2 M KI in the catholyte is depicting a different scenario after

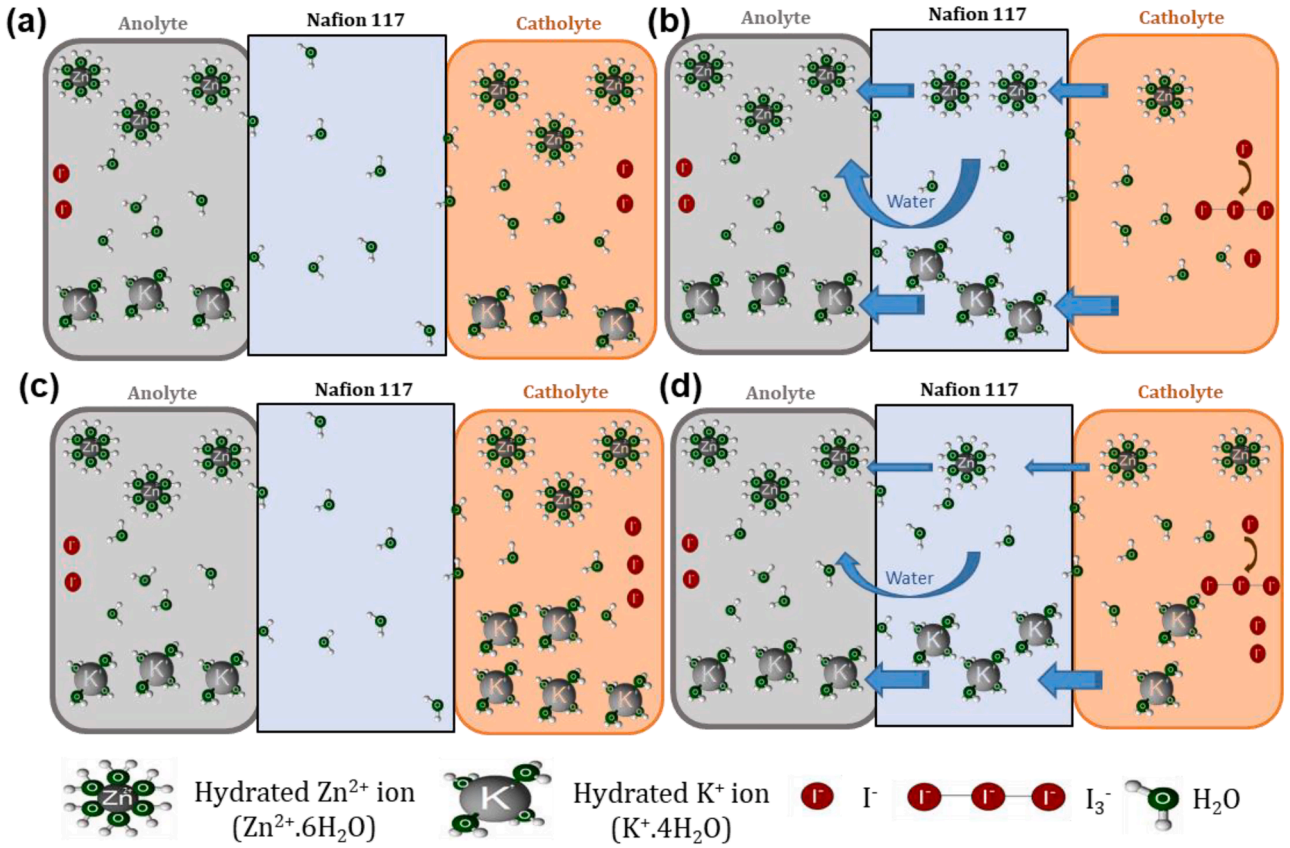

Fig. 4. Schematic illustration of cations migration mechanism following water transfer through Nafion 117 CEM in charge process of electrolytes consisting of 1.5 M ZnI_2: KI (1:1) at before charge (a), after charge (b), and 1.5 M ZnI_2: KI (1:1) + 2 M $KI_{catholyte}$, before charge (c) and after charge (d).

charge, with around 66% of K^+ and 32% of Zn^{2+} ions migrated from catholyte to anolyte during charge. For better understanding, schematic illustrations of ion transport resulting in water transfer phenomena through the membrane before and after charge, are explained in Fig. 4. To sum up, according to our observations, K^+ ions are the dominant migrating cationic species through the membrane, compared to divalent Zn^{2+} ions. In the standard electrolyte, almost all the K^+ ions from the catholyte along with a major portion of Zn^{2+} ions moved to the anolyte while in the tuned electrolyte, comparatively 50% less Zn^{2+} ions migrated due to the availability of more K^+ ions in the catholyte solution.

Several parameters play important roles in cation diffusion and water transport through Nafion membrane. Nightingale et al. compared the hydrated ionic radii of various monovalent and multivalent ions, reporting hydrated Zn^{2+} ions ($Zn^{2+}{\cdot}6H_2O$) of radii 4.3 Å and hydrated K^+ ions ($K^+{\cdot}4H_2O$) of 3.3 Å, respectively [31] These values give a clear view of what we have observed that solvated K^+ ions move faster through the membrane than Zn^{2+} ions because of having higher mobility. Xie and Okada et al. stated that water transport behavior in Nafion 117 is related to parameters like surface-charge density, hydration enthalpy of the cations. After conducting experiments with various aqueous electrolytes containing monovalent and multivalent cations, it has been found that divalent cations exhibit higher charge density and hydration enthalpy [32] hence, tend to carry more water molecules during transport [33]. The study of Goswami et al. about the self-diffusion coefficients of monovalent and divalent cations in Nafion 117 presents that monovalent ions have higher self-diffusion coefficients compared to divalent ions. Consequently, K^+ ions show a higher diffusion coefficient value than Zn^{2+} ions. In addition, they have performed water uptake studies of these various ions in Nafion 117, and the results show lower water uptake capacity by K^+ ions (12.3%) compared to Zn^{2+} ions (21.3%) [34]. All these studies closely match with the results we obtained. In this sense, although divalent Zn^{2+} cations, possess lower self-diffusion coefficients and slower mobility than K^+ ions, can transport more water molecules through the membrane, due to their higher water uptake, being major responsible for water migration. Now, the comparison of the link between the ions and water transport scheme through the membrane of the two sets of electrolytes we have studied is very clear: in the standard electrolyte, after the migration of almost all hydrated K^+ ions, a major portion of Zn^{2+} ions along with large water molecules migrate from catholyte to anolyte, causing larger volume variation; whereas due to the availability of more K^+ ions in the tuned electrolyte, almost ~50% less Zn^{2+} ions migrated which significantly suppresses the water migration.

Finally, the total number of moles and the total molar ion concentrations depict the complete picture of the standard and tuned electrolyte system, showing much higher total molar concentrations in anolyte compared to catholyte in case of standard electrolyte whereas the difference is comparatively very less in the tuned electrolyte. Comparison of these practical values of molar concentrations with the detailing, given in the theoretical calculation (Table S1 for standard electrolyte) and (Table S2 for tuned electrolyte), makes a close correlation that balancing the total ions concentrations of half-cell electrolytes by addition of extra solute to the compartment of lower solute concentrations (catholyte in this case) is an efficient way to suppress the water crossover through the membrane which is an effect of differential ions concentrations.

3.4. Electrochemical performance

Fig. 5 shows the comparison of the first cycle of the charge-discharge profile of ZIFB single cell, carried out with these two sets of electrolytes at a current density of 10 mA·cm^{-2}. The cell with tuned electrolyte is exhibiting better performance with higher discharge capacity and lower internal resistance compared to the cell with standard electrolyte. During the charge, R_{ohm} of the full ZIFB single cell was estimated from the

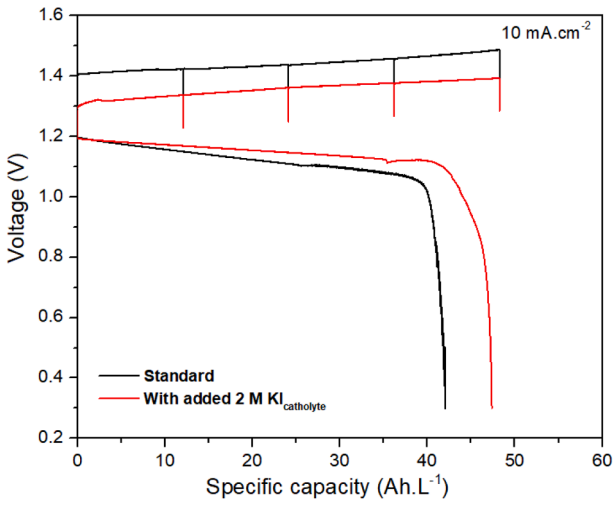

Fig. 5. Comparison of 1st cycle charge-discharge voltage curves of the ZIFB single cell with the electrolyte of without and with added 2 M KI in catholyte at a current density of 10 mA·cm^{-2}. During the charge, at every 15% SOC, EIS measurements were carried out at open-circuit-voltage.

current-interrupt method (Fig. S7 and Table S6). It is interesting to mention that, compared to the cell consisting of standard electrolyte, the cell with tuned electrolyte exhibits on an average of 100 mV magnitude of lower polarization voltage following a stable R_{ohm}, associated with the lowest voltage drop after relaxation throughout the different SOCs. These stable and lowest values of R_{ohm} of the cell agree with the stable catholyte R_{ohm} values obtained from EIS analyses (Fig. 3b) together with the restriction of Zn^{2+} migration though the membrane as seen ICP analysis. These R_{ohm} values could give a preliminary idea about the electrical conductivity of the cell which is higher in the case of the asymmetric formulation. Cycling performance at 10 mA·cm^{-2} is shown in Fig. S8, indicating that, besides the first cycle, the current efficiency slightly improves after the 6th cycle with added 2 M KI.

In summary, these comparisons of half-cell electrolyte conductivity following full-cell electrical conductivities with standard and tuned electrolytes, add another parallel statement of our present study of electrolytes volume imbalances of ZIFB. The cell operating with balanced electrolytes concentrations not only suppressed the water crossover but also improved the cell conductivity and performance.

4. Conclusion

In this study, differences of total ions concentrations between half-cell charged electrolytes is proposed to be the main underlying factor for neutralizing water migration caused by water transport from the compartment of lower (catholyte) to higher (anolyte) ions concentrations via osmosis phenomenon, which is a serious issue since it hinders RFBs from full-fledged commercialization.

Balancing the total ions concentrations of both sides electrolyte chambers, by the addition of extra solute (KI) to the chamber of lower molar concentration (catholyte in this case) has been suggested as a reliable solution of suppressing the water migration.

This hypothesis has been successfully demonstrated experimentally starting from the volume evaluation of ZIFB cell after 1st charge and post-cycling electrolytes. Moreover, analysis of water and ions transport mechanism through Nafion 117 membrane reports K^+ ions are the dominant migrating ion, the addition of extra KI in the catholyte could reduce the passage of large solvated Zn^{2+} ions resulting in higher portion of water transfer. Furthermore, from the stable charged catholyte ohmic resistances from EIS analysis and improved cell electrical conductivity, consequently, better charge-discharge performance confirmed the overall positive impact of ZIFB cell cycling with the

electrolyte of balanced molar concentrations.

This approach, by formulating the electrolytes with the only addition of extra solute ions of the same solution chemistry, to suppress water migration though a cationic membrane while maintaining the classical flow battery format, can positively add a valuable point to the commercialization of the next-generation flow batteries.

CRediT authorship contribution statement

Monalisa Chakraborty: Investigation, Formal analysis, Data curation, Writing – original draft. **Teresa Andreu:** Conceptualization, Methodology, Validation, Resources, Data curation, Writing – review & editing, Project administration, Funding acquisition. **Ben Molinari:** Investigation, Formal analysis. **Joan R. Morante:** Conceptualization, Methodology, Funding acquisition. **Sebastián Murcia-López:** Conceptualization, Methodology, Resources, Writing – review & editing, Visualization, Supervision, Project administration.

Declaration of Competing Interest

The authors declare that they have no known competing financial interests or personal relationships that could have appeared to influence the work reported in this paper.

Data availability

Data will be made available on request.

Acknowledgments

The authors thank Generalitat de Catalunya for financial support through the CERCA Program, projects 2021SGR00712 and 2021SGR01581. IREC also acknowledges support by the European Regional Development Funds (ERDF, FEDER) and by MINECO project WINCOST ENE2016-80788-C5-5-R and MCIN/AEI/10.13039/501100011033 projects PID2019-108136RB-C33 and PID2020-116093RB-C42. M.C. has received her Ph.D. funding from the European Union's Horizon 2020 research and innovation programme under the Marie Skłodowska-Curie grant agreement No 754397. M.C. acknowledges her Doctorate programme, 'Programa de Doctorat en Ciència de Materials de la UAB'. Authors thank Dr. Jordi Jacas Biendicho for fruitful discussions about EIS data analysis. Authors thank Centres Científics i Tecnològics (CCiTUB), Universitat de Barcelona for providing the ICP-OES equipment facility, and Dr. Maite Romero for conducting the measurement.

Supplementary materials

Supplementary material associated with this article can be found, in the online version, at doi:10.1016/j.electacta.2023.142660.

References

[1] J.A. Turner, A realizable renewable energy future, Science 285 (1999) 687–689, https://doi.org/10.1126/science.285.5428.687.
[2] A.Z. Weber, M.M. Mench, J.P. Meyers, P.N. Ross, J.T. Gostick, Q. Liu, Redox flow batteries: a review, J. Appl. Electrochem. 41 (2011) 1137–1164, https://doi.org/10.1007/s10800-011-0348-2.
[3] G.L. Soloveichik, Flow batteries: current status and trends, Chem. Rev. 115 (2015) 11533–11558, https://doi.org/10.1021/cr500720t.
[4] M. Skyllas-Kazacos, M.H. Chakrabarti, S.A. Hajimolana, F.S. Mjalli, M. Saleem, Progress in flow battery research and development, J. Electrochem. Soc. 158 (2011) R55, https://doi.org/10.1149/1.3599565.
[5] M. Skyllas-Kazacos, M. Rychcik, R.G. Robins, A.G. Fane, M.A. Green, New all-vanadium redox flow cell, J. Electrochem. Soc. 133 (1986) 1057–1058, https://doi.org/10.1149/1.2108706.
[6] M. Skyllas-Kazacos, F. Grossmith, Efficient vanadium redox flow cell, J. Electrochem. Soc. 134 (1987) 2950–2953, https://doi.org/10.1149/1.2100321.
[7] Á. Cunha, J. Martins, N. Rodrigues, F.P. Brito, Vanadium redox flow batteries: a technology review, Int. J. Energy Res. 39 (2015) 889–918, https://doi.org/10.1002/ER.3260.
[8] K. Lourenssen, J. Williams, F. Ahmadpour, R. Clemmer, S. Tasnim, Vanadium redox flow batteries: a comprehensive review, J. Energy Storage 25 (2019), 100844, https://doi.org/10.1016/J.EST.2019.100844.
[9] Z. Yuan, Y. Yin, C. Xie, H. Zhang, Y. Yao, X. Li, Advanced materials for zinc-based flow battery: development and challenge, Adv. Mater. 31 (2019), 1902025, https://doi.org/10.1002/ADMA.201902025.
[10] B. Li, Z. Nie, M. Vijayakumar, G. Li, J. Liu, V. Sprenkle, W. Wang, Ambipolar zinc-polyiodide electrolyte for a high-energy density aqueous redox flow battery, Nat. Comm. 6 (2015) 1–8, https://doi.org/10.1038/ncomms7303.
[11] B. Li, J. Liu, Z. Nie, W. Wang, D. Reed, J. Liu, P. McGrail, V. Sprenkle, Metal-organic frameworks as highly active electrocatalysts for high-energy density, aqueous zinc-polyiodide redox flow batteries, Nano Lett. 16 (2016) 4335–4340, https://doi.org/10.1021/acs.nanolett.6b01426.
[12] G.M. Weng, Z. Li, G. Cong, Y. Zhou, Y.C. Lu, Unlocking the capacity of iodide for high-energy-density zinc/polyiodide and lithium/polyiodide redox flow batteries, Energy Environ. Sci. 10 (2017) 735–741, https://doi.org/10.1039/c6ee03554j.
[13] C. Xie, H. Zhang, W. Xu, W. Wang, X. Li, A long cycle life, self-healing zinc–iodine flow battery with high power density, Angew. Chem. - Int. Ed. 57 (2018) 11171–11176, https://doi.org/10.1002/anie.201803122.
[14] C. Xie, Y. Liu, W. Lu, H. Zhang, X. Li, Highly stable zinc-iodine single flow batteries with super high energy density for stationary energy storage, Energy Environ. Sci. 12 (2019) 1834–1839, https://doi.org/10.1039/c8ee02825g.
[15] S. Ito, M. Sugimasa, Y. Toshimitsu, A. Orita, M. Kitagawa, M. Sakai, Formation of a hydrophobic polyiodide complex during cathodic oxidation of iodide in the presence of propylene carbonate in aqueous solutions, and its application to a zinc/iodine redox flow battery, Electrochim. Acta 319 (2019) 164–174, https://doi.org/10.1016/j.electacta.2019.06.150.
[16] M. Mousavi, H. Dou, H. Fathiannasab, C.J. Silva, A. Yu, Z. Chen, Elucidating and tackling capacity fading of zinc-iodine redox flow batteries, Chem. Eng. J. 412 (2021), 128499, https://doi.org/10.1016/J.CEJ.2021.128499.
[17] Q.P. Jian, M.C. Wu, H.R. Jiang, Y.K. Lin, T.S. Zhao, A trifunctional electrolyte for high-performance zinc-iodine flow batteries, J. Power Sources 484 (2021), 229238, https://doi.org/10.1016/J.JPOWSOUR.2020.229238.
[18] M. Chakraborty, S. Murcia-López, J.R. Morante, T. Andreu, Structural influence of the anode materials towards efficient Zn deposition/dissolution in aqueous Zn-iodide flow batteries, J. Electrochem. Soc. 168 (2021), 040532, https://doi.org/10.1149/1945-7111/ABF4EE.
[19] M. Mousavi, G. Jiang, J. Zhang, A.G. Kashkooli, H. Dou, C.J. Silva, Z.P. Cano, Y. Niu, A. Yu, Z. Chen, Decoupled low-cost ammonium-based electrolyte design for highly stable zinc–iodine redox flow batteries, Energy Storage Mater. 32 (2020) 465–476, https://doi.org/10.1016/J.ENSM.2020.06.031.
[20] J. Zhang, G. Jiang, P. Xu, A. Ghorbani Kashkooli, M. Mousavi, A. Yu, Z. Chen, An all-aqueous redox flow battery with unprecedented energy density, Energy Environ. Sci. 11 (2018) 2010–2015, https://doi.org/10.1039/C8EE00686E.
[21] C. Sun, J. Chen, H. Zhang, X. Han, Q. Luo, Investigations on transfer of water and vanadium ions across Nafion membrane in an operating vanadium redox flow battery, J. Power Sources 195 (2010) 890–897, https://doi.org/10.1016/J.JPOWSOUR.2009.08.041.
[22] K.W. Knehr, E. Agar, C.R. Dennison, A.R. Kalidindi, E.C. Kumbur, A transient vanadium flow battery model incorporating vanadium crossover and water transport through the membrane, J. Electrochem. Soc. 159 (2012) A1446–A1459, https://doi.org/10.1149/2.017209JES/XML.
[23] L. Yan, D. Li, S. Li, Z. Xu, J. Dong, W. Jing, W. Xing, Balancing osmotic pressure of electrolytes for nanoporous membrane vanadium redox flow battery with a draw solute, ACS App. Mater. Interfaces 8 (2016) 35289–35297, https://doi.org/10.1021/ACSAMI.6B12068/SUPPL_FILE/AM6B12068_SI_001.PDF.
[24] K. Oh, M. Moazzam, G. Gwak, H. Ju, Water crossover phenomena in all-vanadium redox flow batteries, Electrochim. Acta 297 (2019) 101–111, https://doi.org/10.1016/J.ELECTACTA.2018.11.151.
[25] Y. Song, X. Li, J. Xiong, L. Yang, G. Pan, C. Yan, A. Tang, Electrolyte transfer mechanism and optimization strategy for vanadium flow batteries adopting a Nafion membrane, J. Power Sources 449 (2020), 227503, https://doi.org/10.1016/J.JPOWSOUR.2019.227503.
[26] X. Liu, H. Zhang, Y. Duan, Z. Yuan, X. Li, Effect of electrolyte additives on the water transfer behavior for alkaline zinc-iron flow batteries, ACS Appl. Mater. Interfaces 12 (2020) 51573–51580, https://doi.org/10.1021/ACSAMI.0C16743/SUPPL_FILE/AM0C16743_SI_001.PDF.
[27] C. Wei, Z.J. Xu, C. Wei, Z.J. Xu, The comprehensive understanding of as an evaluation parameter for electrochemical water splitting, Small Methods 2 (2018), 1800168, https://doi.org/10.1002/SMTD.201800168.
[28] Y.A. Gandomi, D.S. Aaron, J.R. Houser, M.C. Daugherty, J.T. Clement, A. M. Pezeshki, T.Y. Ertugrul, D.P. Moseley, M.M. Mench, Critical review—experimental diagnostics and material characterization techniques used on redox flow batteries, J. Electrochem. Soc. 165 (2018) A970–A1010, https://doi.org/10.1149/2.0601805JES/XML.
[29] J.D. Jeon, H.S. Yang, J. Shim, H.S. Kim, J.H. Yang, Dual function of quaternary ammonium in Zn/Br redox flow battery: capturing the bromine and lowering the charge transfer resistance, Electrochim. Acta 127 (2014) 397–402, https://doi.org/10.1016/J.ELECTACTA.2014.02.073.
[30] F. ShakeriHosseinabad, S.R. Daemi, D. Momodu, D.J.L. Brett, P.R. Shearing, E.P. L. Roberts, Influence of flow field design on zinc deposition and performance in a zinc-iodide flow battery, ACS Appl Mater Interfaces 13 (2021) 41563–41572, https://doi.org/10.1021/ACSAMI.1C09770.

[31] E.R. Nightingale, Phenomenological theory of ion solvation. Effective radii of hydrated ions, J. Phys. Chem. 63 (1959) 1381–1387, https://doi.org/10.1021/J150579A011/ASSET/J150579A011.FP.PNG_V03.
[32] D.W. Smith, Ionic hydration enthalpies, J. Chem. Educ. 54 (1977) 540–542, https://doi.org/10.1021/ED054P540.
[33] G. Xie, T. Okada, Water transport behavior in nafion 117 membranes, J. Electrochem. Soc. 142 (1995) 3057–3062, https://doi.org/10.1149/1.2048686/XML.
[34] A.K. Goswami, A. Acharya, A.K. Pandey, Study of self-diffusion of monovalent and divalent cations in nafion-117 ion-exchange membrane, J. Phys. Chem. B 105 (2001) 9196–9201, https://doi.org/10.1021/JP010529Y.